DEFECTS AND SITE OCCUPANCIES IN Nb-Cr-Ti *C*15 LAVES PHASE ALLOYS

P.G. Kotula, C.B. Carter, K.C. Chen, D.J. Thoma, F. Chu and T.E. Mitchell
Materials Science and Technology Division, MS K765, Los Alamos National Laboratory, Los Alamos, NM 87545

Introduction

Laves-phase intermetallics are of potential use as high-temperature structural materials (1–7). $NbCr_2$-based *C*15-structured alloys are of particular interest for such applications (4,7). The effect of Ti additions to $NbCr_2$ on the microstructure and mechanical properties of such alloys has been investigated and Ti has been shown to improve the fracture toughness of the monolithic *C*15 Laves phase (8) and dual-phase (bcc + *C*15) alloys (9–11). The particular site occupancy of the ternary alloy elements has been proposed to have significant effects on the synchroshear deformation mechanism (5,12,13). Thus, strategic alloying may improve the brittleness normally associated with Laves phases.

In the Nb-Cr-Ti system, there is a complete solid solution between $NbCr_2$ and $TiCr_2$ with a significant range of solubility for the *C*15 phase and a large two-phase region of bcc and *C*15 (8,14). The Nb-Cr-Ti phase diagram (950°C isothermal section) is shown in Figure 1. The initial characterization by transmission electron microscopy (TEM) of the defect structure of an alloy of overall composition $Nb_{10}Cr_{75}Ti_{15}$ is discussed here. Additionally, Atom Location by CHanneling Enhanced MIcroanalysis (ALCHEMI) (15) was employed to examine the site occupancies of the Nb, Cr and Ti in this *C*15 Laves phase.

Experimental

$Nb_{10}Cr_{75}Ti_{15}$ was prepared by arc-melting the high-purity elemental metals followed by annealing in an evacuated and backfilled (high-purity argon) furnace at 1400°C for 120 h (slow furnace cooled, 1°C/min). Specimens were prepared for observation in the TEM by cutting 3 mm discs with a coring saw, followed by dimpling and ion milling. Microstructural characterization was performed by TEM with a Philips CM30 operating at 300 kV. The composition of the Laves phase was measured by energy-dispersive x-ray (EDX) analysis in the TEM using the Cliff-Lorimer ratio technique. Microprobe measurements were made of both bcc and *C*15 Laves phases from equilibrated Nb-$NbCr_2$ and Ti-$TiCr_2$ alloys from which the k-factors, k_{NbCr} and k_{TiCr}, were determined. The final k-factors were the average of those from the bcc and Laves phases for the given alloy: $k_{NbCr} = 1.69 \pm 0.02$ and $k_{TiCr} = 1.00 \pm 0.02$. All of the spectra for compositional analysis of the C15 Laves phases were collected well away from strongly channeling diffracting conditions to avoid the ALCHEMI effect. For the ALCHEMI experiments, EDX spectra were acquired near <014> over a range of {400} excitations between symmetry and beyond {12 0 0}. Spectra were also acquired near <334> over a range of {440}

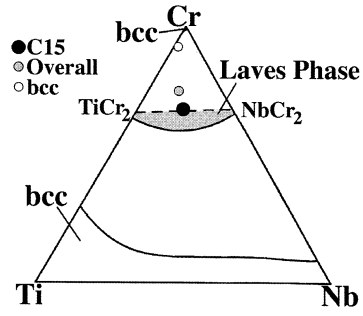

Figure 1. Nb-Cr-Ti phase diagram (950°C isothermal section) (8).

excitations between symmetry and {880}. Site-distributions were extracted from the data by multivariate statistical analysis (MSA) (16) with delocalization correction (17) as described elsewhere (18,19).

Results and Discussion

The composition of the *C*15 Laves phase was measured by EDX on the TEM to be $Nb_{15}Ti_{17}Cr_{68}$. The filled gray circle in Figure 1 is the starting composition of the alloy, the filled black circle is the measured composition of the *C*15 Laves phase. The open circle is the measured composition of the Cr-rich bcc phase. The overall composition of the alloy should lie on a straight line between the bcc and *C*15 phases. However, owing to the extended solubility of the Cr-rich solid solution and the observation of a small amount of a Ti-rich phase, a completely equilibrated phase distribution may not have been achieved in this alloy. Figure 2 shows the variation of the delocalization-corrected x-ray intensity ratios with orientation for $Nb_{15}Cr_{68}Ti_{17}$. MSA indicated a $91.1 \pm 1.6\%$ correlation between Nb and Ti. The results are consistent with all of the Ti atoms occupying the A sublattice (as in $TiCr_2$) with the Nb atoms partitioning between the A and B sites and all of the Cr atoms on the B site. Assuming no Ti-Cr anti-site defects the Laves phase would be $(Nb_{14}Ti_{17})_A[Cr_{68}Nb_1]_B$. This agrees with the AB_2 stoichiometry to within the error of the microanalysis results.

Figure 3a is a 'weak-beam' dark-field ('WB'DF) TEM image of a multiply-faulted dipole with the fault planes inclined to the beam. The foil normal was near $[\bar{1}2\bar{1}]$, the beam direction, **B** (upward pointing direction with respect to the sample) was near $[\bar{1}\bar{1}\bar{1}]$ and $\mathbf{g}(02\bar{2})$ was used to form the image with 4.5**g** excited ($s = 0.056\ nm^{-1}$). The imaging conditions utilized were not 'true' weak-beam conditions as defined by Cockayne, Ray and Whelan (20). However, for the analysis described in this

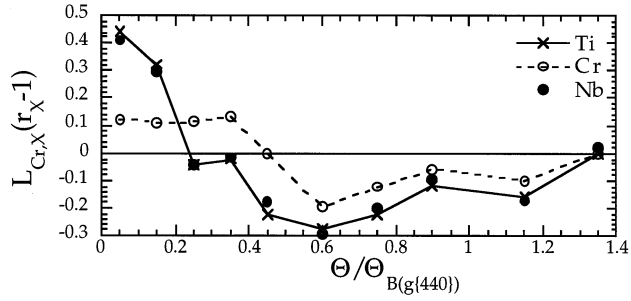

Figure 2. Variation of the delocalization-corrected x-ray intensity ratios for $Nb_{15}Cr_{68}Ti_{17}$ with orientation along the {440} systematic row.

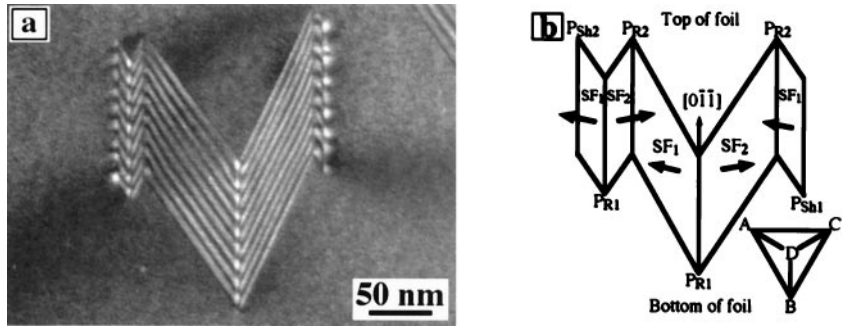

Figure 3. (a) 'WB'DF TEM image of a multiply-faulted dipole. (b) Schematic of (a). P_{Sh1} and P_{Sh1} are Shockley partials, P_{R1} and P_{R2} are stair-rod dislocations and SF_1 and SF_2 are stacking faults. Inset is the Thompson tetrahedron.

paper, 'true' weak-beam conditions are not essential. Figure 3b is a schematic of Fig. 3a showing the fault planes and partial dislocations. The Thompson tetrahedron is inset.

Figure 4a is a bright-field TEM image taken with **B** near [0$\bar{1}\bar{1}$] so that the faults and partial dislocations are nearly end on. All of the partials have a line direction of [011] and the fault planes are shown in the schematic in Fig. 4b. When the defect was tilted exactly edge on as shown in Figure 4c (i.e., to **B** = [0$\bar{1}\bar{1}$]) there was no residual contrast from any of the dislocations indicating that they are pure edge in character. The selected-area diffraction (SAD) pattern from [0$\bar{1}\bar{1}$] is shown in Figure 4d. The fault plane, for SF_1, which is the stacking fault adjacent to the two Shockley partials, is ($\bar{1}\bar{1}$1) while that for SF_2 is ($\bar{1}$1$\bar{1}$). This would imply that the Burgers vectors for the Shockley partials, $\mathbf{b}_{Sh}$, are

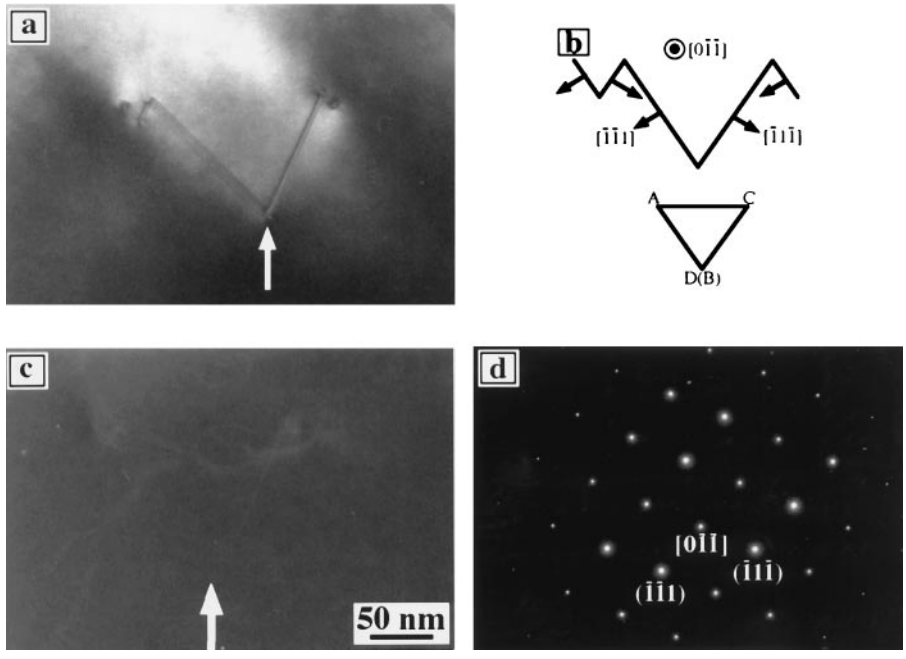

Figure 4. BF TEM of the same defect as in 3(a) viewed nearly edge on. (b) Schematic of (a). (c) BF TEM image taken on [0$\bar{1}\bar{1}$] showing no residual contrast from the dislocations. The arrows in (a) and (c) mark the same part of the defect. (d) SAD pattern on [0$\bar{1}\bar{1}$].

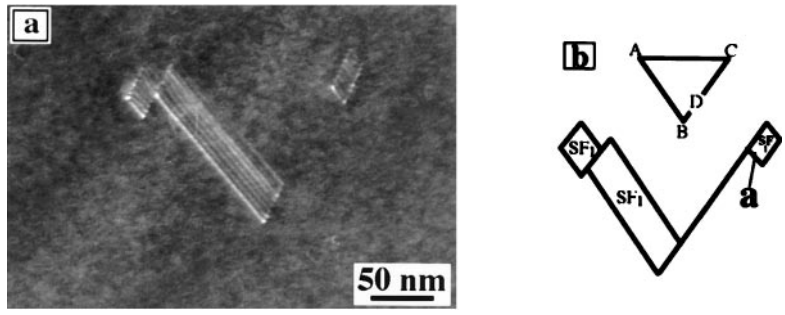

Figure 5. (a) 'WB'DF TEM image used to determine the stacking-fault energy. (b) Schematic of (a).

$\pm 1/6[2\bar{1}1]$ and those for the stair-rods, $\mathbf{b}_R$, are $\pm 1/6[0\bar{1}1]$. From Fig. 3a, it is clear that the stair rods, P_{R1} and P_{R2}, which have **b** of opposite sign, show different contrast. A $\mathbf{g} \cdot \mathbf{b}$ analysis of the defect is consistent with the assignment of Burgers vectors for the partial dislocations described above.

Since the Shockley partials are glissile, and given the Burgers vectors assignment from above, the stacking fault energy, γ, was determined. Figure 5a is a 'WB'DF TEM image with $\mathbf{g}(\bar{2}2\bar{2})$, $3\mathbf{g}$ ($s = 0.048\ nm^{-1}$, $\mathbf{B} \sim [\bar{2}\bar{3}\bar{1}]$). In this case, the foil has been tilted along the $[\bar{1}1\bar{1}]$ Kikuchi band toward the $[\bar{1}\bar{2}\bar{1}]$ zone axis. The partial dislocations show weak contrast while the contrast from SF_1 is prominent. The width of SF_1 at region 'a' (marked in the schematic Fig. 5b), measured in the $[\bar{1}11]$ direction thus gives the separation, Δ, between the Shockley partial (P_{Sh1}) and the stair-rod (P_{R2}); thus the stacking-fault energy was calculated from (20):

$$\gamma = \frac{\mu}{2\pi\Delta}\left(\frac{(\mathbf{b}_2 \times \boldsymbol{\xi}_2) \cdot (\mathbf{b}_3 \times \boldsymbol{\xi}_3)}{(1-\nu)}\right) \tag{1}$$

where $\mathbf{b}_2$ is $1/6[2\bar{1}1]$ and $\mathbf{b}_3$ is $1/6[0\bar{1}1]$ and the line direction of all the dislocations, $\boldsymbol{\xi}$, was parallel to [011]. Δ was measured to be 15 nm from which γ was determined to be 35 mJ/m^2. Isotropic elasticity was assumed with values of the shear modulus ($\mu = 79.6$ GPa) and Poisson's ratio ($\nu = 0.34$) taken from room temperature measurements of $NbCr_2$ (22). The measured value of γ from this work can be compared with experimental (25 mJ/m^2) (23) and theoretical (upper bound of 90 mJ/m^2) (24) studies of $NbCr_2$. The spacing of the partials (P_{Sh2} and P_{R1} from Fig. 3b) at the other end of the defect is 20 nm because of additional repulsion from the nearby stair-rod dislocation (denoted P_{R2} in Figure 3b).

Conclusions

A multiply-faulted dipole in the *C*15 Laves phase of composition $Nb_{15}Cr_{68}Ti_{17}$ has been characterized. The dislocations all lie along [011] and show no residual contrast when imaged edge-on at $\mathbf{B} = [0\bar{1}\bar{1}]$ indicating that they are edge in character. Given this, the Burgers vectors for the Shockley partials are $\pm 1/6[2\bar{1}1]$ and those of the stair-rods are $\pm 1/6[0\bar{1}1]$. This is consistent with a $\mathbf{g} \cdot \mathbf{b}$ analysis which was performed. The stacking fault energy was determined to be 35 mJ/m^2 which is higher than the experimental value of 25 mJ/m^2 from $NbCr_2$ (23). Simulations are currently underway to understand, given the site occupancies and observed trend in stacking fault energy, whether Ti would be expected to raise the stacking fault energy of the *C*15 Laves phase.

ALCHEMI indicates that Ti atoms occupy only the A site in AB_2 while Nb partitions to both sites (mostly to the A site) and Cr occupies only the B site. In this case, the smaller Ti atoms prefer the A site, displacing some Nb to the B site which is normally occupied solely by the smaller Cr atoms. From a geometrical standpoint, Nb and Ti have similar atomic radii (1.468 and 1.462Å respectively) and so

would be expected to predominantly occupy the A site. If some of the A-site atoms were to be displaced to the B site, the smaller Ti atoms would be expected to be moved. As this is not observed, electronic contributions are likely playing a significant role in determining the site occupancies. In the $NbCr_2$-V system, from geometric arguments alone, V atoms should occupy both sublattices, but experimentally it is found that V atoms occupy only the B site with the Cr atoms. This has been explained by electronic-structure arguments (25) and it is likely that similar arguments apply to the *C*15 Laves phases in the Nb-Cr-Ti system.

Acknowledgments

Research at Los Alamos National Laboratory (LANL) was sponsored by the Laboratory Directed Research and Development (LDRD) program and the US Department of Energy (DOE)-OBES. PGK acknowledges a Director-Funded Postdoctoral Fellowship from LANL. CBC acknowledges the Bernd T. Mattias Scholar award from the Center for Materials Science at LANL. The ALCHEMI experiments were performed at Oak Ridge National Laboratory (ORNL) SHaRE User Facility which is sponsored by the Division of Materials Sciences, US Department of Energy under contract DE-AC05-96OR22464 with Lockheed Martin Energy Research Corporation. The assistance of Drs. Ian M. Anderson and James Bentley, at ORNL, with that work is greatly appreciated.

References

1. J. D. Livingston, Phys. Stat. Sol. A. 131, 145 (1992).
2. R. L. Fleischer and R. J. Zabala, Met. Trans. A. 21A, 2149 (1990).
3. M. Takeyama and C. T. Liu, Mater. Sci. Eng. A132, 61 (1991).
4. D. J. Thoma and J. H. Perepezko, Mater. Sci. Eng. A156, 97 (1992).
5. F. Chu and D. P. Pope, Mater. Sci. Eng. A170, 39 (1993).
6. K. S. Kumar and D. B. Miracle, Intermetallics. 2, 257 (1994).
7. T. Takasugi, M. Yoshida, and S. Hanada, Acta Mater. 44, 669 (1996).
8. D. J. Thoma, Ph.D. Thesis, University of Wisconsin, Madison, WI (1992).
9. D. L. Davidson, K. S. Chan, and D. L Anton, Metall. Mater. Trans. 27A, 3007 (1996).
10. D. L. Davidson, Metall. Mater. Trans. 28A, 1297 (1997).
11. K. C. Chen, D. J. Thoma, P. G. Kotula, F. Chu, C. M. Cady, G. T. Gray III, P. S. Dunn, and D. R. Korzekwa, in Proceedings of the 3rd Pacific Rim International Conference on Advanced Materials and Processing (1998), in press.
12. J. D. Livingston and E. L. Hall, J. Mater. Res. 5, 5 (1990).
13. K. C. Chen, S. M. Allen, and J. D. Livingston, Mater. Sci. Eng. 242, 163 (1998).
14. D. J. Thoma and J. H. Perepezko, in Experimental Methods of Phase Diagram Determination, ed. J. E. Morral, R. S. Schiffman, and S. M. Merchant, p. 45, TMS, Warrendale, PA (1994).
15. J. C. H. Spence and J. Taftø, J. Microsc. 130, 147 (1983).
16. C. J. Rossouw et al., Phil. Mag. Lett. 60, 225 (1989).
17. M. G. Walls, Microsc. Microanal. Microstruct. 3, 443 (1992).
18. I. M. Anderson and J. Bentley, in Proceedings of the 13th ICEM: Electron Microscopy 1994, 1, 609 (1994).
19. I. M. Anderson and J. Bentley, in Proceedings of EMAG 95. Bristol: Institute of Physics Conference, 147 (1995).
20. D. J. H. Cockayne, I. L. F. Ray, and M. J. Whelan, Phil. Mag. 20, 1265 (1969).
21. J. P. Hirth and J. Lothe, Theory of Dislocations, Wiley, New York (1982).
22. F. Chu, Y. He, D. J. Thoma, and T. E. Mitchell, Scripta Metall. Mater. 33, 1295 (1995).
23. A. V. Kazantis, M. Aindow, and I. P. Jones, Phil. Mag. Lett. 74, 129 (1996).
24. F. Chu, A. H. Ormeci, T. E. Mitchell, J. M. Wills, D. J. Thoma, R. C. Albers, and S. P. Chen, Phil. Mag. Lett. 72, 147 (1995).
25. F. Chu, D. J. Thoma, P. G. Kotula, S. Gerstl, and T. E. Mitchell, Acta Mater. in press (1998).